



RESEARCH LETTER

10.1002/2014GL060490

Key Points:

- Our combined approach allows separating different causes for seismic anisotropy
- Seismic anisotropy is dominated by crystallographic preferred orientation
- The novel EBSD-based FE simulation has several advantages discussed in the paper

Supporting Information:

- Readme
- Text S1
- Text S2
- Animation S1

Correspondence to:

X. Zhong,
xin.zhong@erdw.ethz.ch

Citation:

Zhong, X., M. Frehner, K. Kunze, and A. Zappone (2014), A novel EBSD-based finite-element wave propagation model for investigating seismic anisotropy: Application to Finero Peridotite, Ivrea-Verbano Zone, Northern Italy, *Geophys. Res. Lett.*, 41, 7105–7114, doi:10.1002/2014GL060490.

Received 20 AUG 2014

Accepted 4 OCT 2014

Accepted article online 7 OCT 2014

Published online 27 OCT 2014

A novel EBSD-based finite-element wave propagation model for investigating seismic anisotropy: Application to Finero Peridotite, Ivrea-Verbano Zone, Northern Italy

Xin Zhong^{1,2}, Marcel Frehner¹, Karsten Kunze³, and Alba Zappone^{4,5}

¹Geological Institute, ETH Zurich, Switzerland, ²Now at Institute of Geochemistry and Petrology, ETH Zurich, Switzerland, ³Scientific Center for Optical and Electron Microscopy, ETH Zurich, Switzerland, ⁴Swiss Seismological Service, ETH Zurich, Switzerland, ⁵Institute of Process Engineering, ETH Zurich, Switzerland

Abstract A novel electron backscatter diffraction (EBSD) -based finite-element (FE) wave propagation simulation is presented and applied to investigate seismic anisotropy of peridotite samples. The FE model simulates the dynamic propagation of seismic waves along any chosen direction through representative 2D EBSD sections. The numerical model allows separation of the effects of crystallographic preferred orientation (CPO) and shape preferred orientation (SPO). The obtained seismic velocities with respect to specimen orientation are compared with Voigt-Reuss-Hill estimates and with laboratory measurements. The results of these three independent methods testify that CPO is the dominant factor controlling seismic anisotropy. Fracture fillings and minor minerals like hornblende only influence the seismic anisotropy if their volume proportion is sufficiently large (up to 23%). The SPO influence is minor compared to the other factors. The presented FE model is discussed with regard to its potential in simulating seismic wave propagation using EBSD data representing natural rock petrofabrics.

1. Introduction

Seismic anisotropy is commonly assumed to be dominantly affected by the petrofabrics, such as the crystallographic preferred orientation (CPO), of volumetrically significant mineral phases, such as quartz in the crust and olivine in the upper mantle [e.g., *Nicolas and Christensen, 1987; Holbrook et al., 1992; Ismail and Mainprice, 1998; Tatham et al., 2008; Lloyd et al., 2011a, 2011b*], or less volumetrically dominant but highly anisotropic minerals like mica [*Llana-Funez and Brown, 2012; Cholach et al., 2005*]. A conventional method to investigate seismic anisotropy from rock samples involves the calculation of Voigt-Reuss-Hill (VRH) averages of the elastic tensor from the single crystal stiffness matrix of the rock forming minerals, weighted by CPO and modal composition [e.g., *Mainprice, 1990; Mainprice and Humbert, 1993; Erdman et al., 2013; Llana-Funez et al., 2009*]. This method calculates seismic anisotropy derived from CPO but does not take into account properties such as shape preferred orientation (SPO) and fracture orientations. Attempts to include these parameters into the simulations have been made using numerical techniques like asymptotic expansion homogenization (AEH) finite-element (FE) theory by calculating the bulk elastic tensor considering grain shape distribution [*Naus-Thijssen et al., 2011*]. Alternative analytical solutions use differential effective medium methods (DEM) by assuming a homogeneous matrix and a pre-defined orientation distribution of highly anisotropic mineral grains, like mica or serpentine [*Nishizawa and Yoshino, 2001; Watanabe et al., 2014*]. In this study, an alternative numerical method is proposed that incorporates digitized EBSD data into a FE model to allow elastic waves to propagate through a fully anisotropic and heterogeneous rock model representing the real petrofabrics in a sample. Such a method not only allows a direct visualization of wave propagation but also provides full control on the different factors responsible for seismic anisotropy, such as the separation of CPO and SPO as demonstrated in this study.

To test the proposed model, we carried out direct laboratory measurements of ultrasonic wave propagation on peridotite samples collected from Finero, Ivrea-Verbano Zone, using the pulse transmission technique, and comparing the results with VRH calculations and with the new numerical FE simulations. The Finero peridotite massif is an ultramafic lens outcropping at the northernmost end of the Ivrea-Verbano Zone, in Northern Italy [e.g., *Lensch, 1968; Coltorti and Siena, 1984; Rutter et al., 2007*]. It is mainly composed of

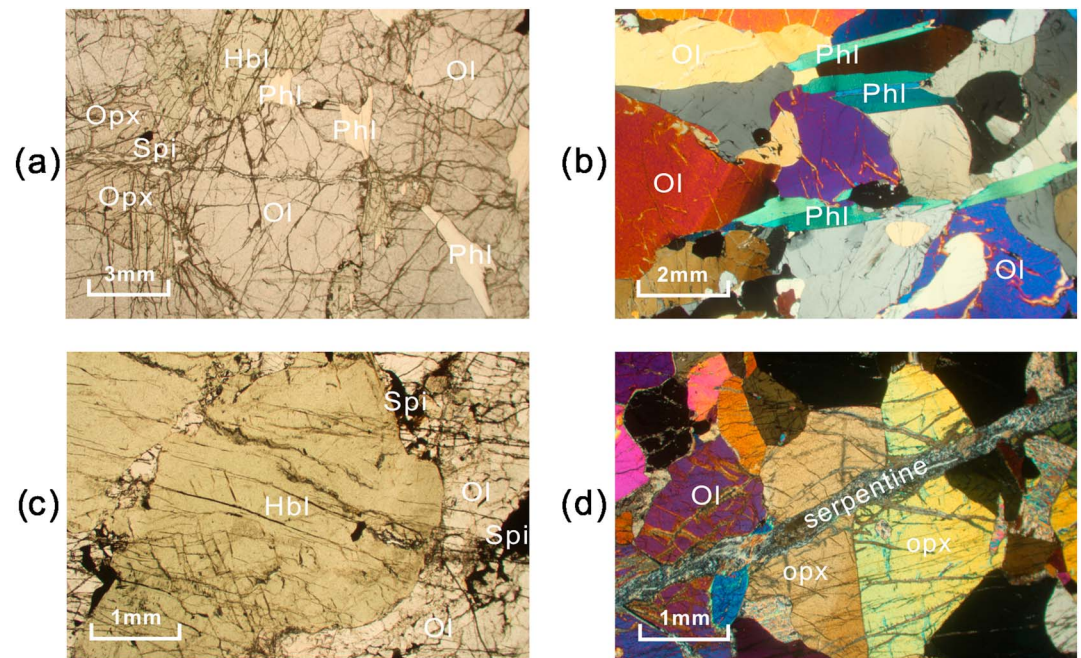


Figure 1. Optical microscopic images of Finero peridotite (Ol = olivine; Opx = orthopyroxene; Phl = phlogopite; Hbl = hornblende; Spi = spinel). (a) General view of the massive rock microscopy. (b) and (c) Preferentially aligned phlogopite and a large hornblende crystal respectively. (d) Fracture filled with serpentine from sample ZAP205. Figures 1a–1c are photographed from a rock collection of Finero peridotite. Lineation is defined by the preferentially aligned olivine and phlogopite. The modal percentages of different phases are given in Figure 3 together with the calculated Hill averaged velocity of individual phases and the bulk rock. The crystallographic preferred orientations in form of stereograms are in the supporting information. Note that a fracture is filled with serpentine in Figure 1d, which is also observed in the electron backscatter diffraction (EBSD) image (Figure 2). The serpentine grains in the fracture are ultrasmall and randomly orientated based on their dark birefringence and reaction rims beside the olivine grains.

harzburgites and lherzolites that suffered intense metasomatic enrichment, resulting in the pervasive presence of amphibole and phlogopite and locally apatite and carbonates. According to *Siena and Coltorti* [1989], the mafic-ultramafic complex experienced maximum pressure and temperature conditions of about 1 GPa and 1000°C. Given the easy accessibility to the zone, the excellent quality of the outcrops, and the absence of pervasive retrograde metamorphism or tectonic overprint, the Ivrea-Verbano Zone has been intensely studied, and it has frequently been used as a model to help interpret features of deep crustal seismic profiles [e.g., *Fountain*, 1976; *Rudnick and Fountain*, 1995; *Holliger et al.*, 1993; *Holliger and Levander*, 1994; *Rutter et al.*, 1999; *Khazanehdari et al.*, 2000]. In this study, we use a comprehensive approach involving laboratory measurements, VRH calculations, and EBSD-based FE simulations to address the origin of observed seismic anisotropy with particular focus on the influence of CPO and SPO, as well as fractures at thin section scale.

2. Materials and Methodology

2.1. Sample Description

Two phlogopite-bearing harzburgites (samples ZAP205 and ZAP214) have been selected from a wider sample collection of ultramafites from the Finero massif to present the proposed approach in the present work. The microstructure and mineralogical composition of the selected samples are presented in Figure 1. In these peridotites the amphibole modal concentration exceeds that of clinopyroxene; the two selected samples differ in amphibole content (3.98% in ZAP205 and 23.94% in ZAP214). In both samples, olivine and sometimes orthopyroxene display metamorphic deformations (kink bands, Figure 1b), which are absent in the clinopyroxene crystals. Large phlogopite crystals define a foliation and cut through all the other phases. Amphibole grains are preferentially aligned and define the lineation in sample ZAP214 observed

from hand specimen. Secondary minerals are mainly limited to disseminated oxides and serpentine localized in microfractures. Serpentine fibers are randomly oriented within the fractures (Figure 1).

2.2. Electron Backscatter Diffraction

Crystal orientation mapping by means of EBSD is a powerful tool to acquire information on the micro-texture of polycrystalline and poly-phase rocks [Adams *et al.*, 1993; Prior *et al.*, 1999; Schwartz *et al.*, 2009]. The EBSD technique has also been used to study CPO and its relationship to seismic anisotropy in mafic-ultramafic rocks such as peridotite and eclogite [Mauler *et al.*, 2000; Frese *et al.*, 2003; Wang *et al.*, 2009; Worthington *et al.*, 2013]. The result of an EBSD scan is a 2D map containing spatial information about the mineral phases and their crystallographic orientations. We performed large area scans (about 20 mm by 20 mm) with a step size of 25 μm collecting data on crystal orientation (by EBSD) and mineral composition (by energy dispersive X-ray spectroscopy, EDXS) simultaneously. The employed device is a scanning electron microscope (SEM) EOsCan by Tescan (Brno, CZ) equipped with a Pegasus analytical system by Ametek-EDAX (Mahwah, NJ, USA). Post-processing of the combined data on EBSD patterns and element content was performed using the ChiScan option in the software package OIM 6 (Mahwah, NJ, USA). EBSD patterns were only indexed for the candidate phases compatible with the EDXS element composition to extract the orientation and mineral phase at each pixel of the maps. Non-reliable data points were excluded from subsequent analysis by confidence index filtering.

The VRH estimates of bulk elastic properties are calculated directly from EBSD measurements using standard methodologies, which have been extensively used in seismic anisotropy studies in a wide variety of lithologies [e.g., Burlini and Kunze, 2000; Bascou *et al.*, 2001; Pera *et al.*, 2003; Lloyd and Kendall, 2005; Valcke *et al.*, 2006; Xu *et al.*, 2006; Mainprice *et al.*, 2011]. The Voigt (upper) and Reuss (lower) bounds are the averaged elastic property of a polyphase, polycrystalline aggregate assuming homogeneous strain or stress, respectively [Voigt, 1928; Reuss, 1929]. The Hill average is simply the arithmetic mean of the Voigt and Reuss bounds, thus providing an intermediate estimate for seismic velocity and anisotropy [Hill, 1952]. These models do not include grain boundary conditions, grain interactions, or grain shape. The MTEX MATLAB toolbox is used here to calculate the orientation distribution function (ODF, provided in the supporting information) and stereograms as well as the VRH bounds with input of single crystal elastic tensors and density of mineral phases, and crystallographic orientations at all the mapping positions [Bachmann *et al.*, 2010].

For each XY position in the EBSD scan, the recorded crystal orientation is used to rotate the 3D anisotropic stiffness matrix for the individual single mineral phase [Babuska and Cara, 1991] into the respective crystal orientation [Bachmann *et al.*, 2010; Mainprice *et al.*, 2011]. The rotated 3D stiffness matrices (6-by-6) are reduced to 2D matrices (3-by-3) for further numerical FE simulation performed in 2D (for details see supporting information).

2.3. Numerical Finite-Element Model

The FE method is applied to simulate compressional wave propagation in the fully anisotropic and heterogeneous 2D rock model derived from the EBSD maps. A 2D plane strain formulation of the governing force balance and the linear elastic rheological eqs. are used. The numerical code is derived from the codes presented, benchmarked, and applied in Frehner *et al.* [2008], Frehner and Schmalholz [2010], and Frehner [2014]. The grid of the FE model is in accordance with the square pixels measured by EBSD, and the physical property of each numerical element corresponds to the elastic tensor calculated from the crystallographic orientation and single crystal stiffness matrix (Figure 2). Therefore, our FE model is discretized in the same way as the EBSD measurement in terms of spatial coordinates. The advantage of such a model is that the measured EBSD data are easily processed and implemented into the FE model to allow waves propagating through the digitized rock model affected by petrofabrics and crystallographic orientations. This method bridges EBSD measurements and numerical simulation and provides a simple and straightforward alternative to study seismic anisotropy. Details on the basic equations of force balance and elastic rheology are provided in the supporting information.

Wave propagation is simulated for a series of propagation directions in angles every 10° from 0° to 180°. To do this, the measured EBSD orientation data set is rotated in steps of 10° relative to the center of the model (Figure 2). The source wave is always fixed at the left edge of the model and is prescribed as a Gaussian function. Numerical receivers are implemented on both the left and right edges of the model (Figures 2b and

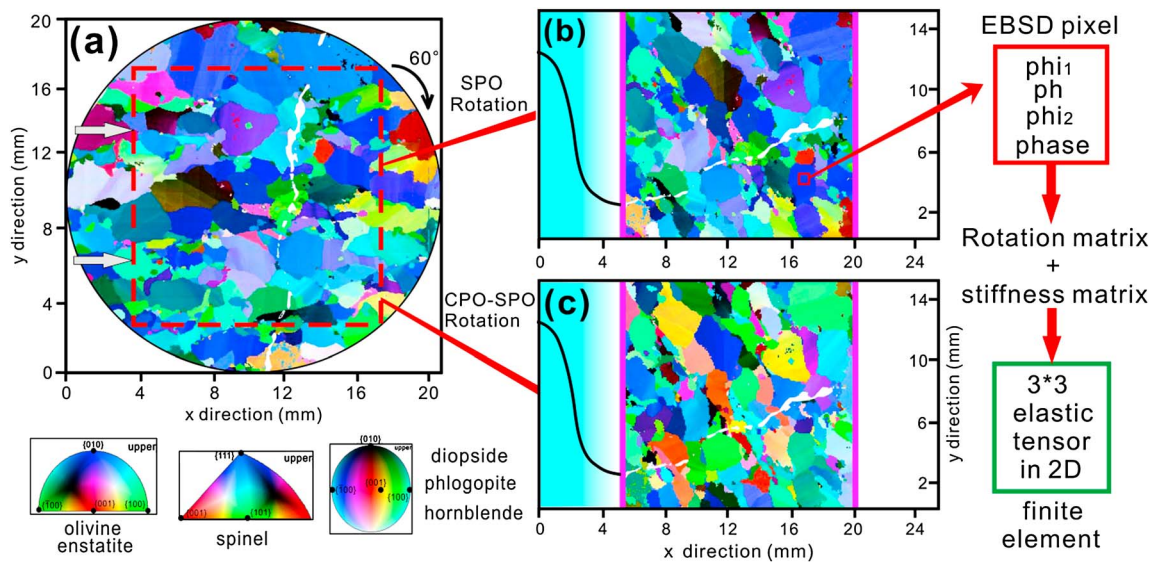


Figure 2. (a) Rock digitization of the EBSD crystallographic orientation map. Color coding of the crystal orientation for all the phases with respect to the sample X-direction is shown at the bottom. The dashed red square is the model frame for finite-element (FE) modeling. Figures 2b and 2c are the 60° rotated *shape preferred orientation (SPO)-rotation model* and *crystallographic preferred orientation-CPO-SPO-rotation model*, respectively. Note that the color indexed grain orientation remains unchanged in the *SPO-rotation model* but changes in the *CPO-SPO rotation model* due to the rotation of the crystallographic orientation. The pink lines are the virtual receivers in the FE simulations to average the displacement field in order to calculate the effective seismic velocity. They are bounded with two isotropic, homogeneous virtual “aluminum transducers” to guarantee a smooth source wave and to avoid disturbance from boundary reflection. The blue shading and the black curves on the left indicate the incident seismic wave (Gaussian function). During digitization, the elastic tensor of each EBSD pixel, such as the small red box in Figure 2b, is calculated using the three Bunge angles (ϕ_1 , ϕ , and ϕ_2) and the original stiffness matrix of the corresponding mineral phase. The result of EBSD digitization is a 2D elastic tensor, which is used in FE model with the same coordinates as measured by EBSD.

2c pink lines) to average the displacement and to calculate the effective seismic velocity. The 2D EBSD orientation map was measured on the XZ plane, i.e., normal to the foliation plane and parallel to the lineation, representing the maximal seismic anisotropy. Therefore, the numerical results correspond to the effective seismic anisotropy, thus represent the bulk rock in 3D and can be compared with VRH estimates and laboratory measurements.

Additional simulations were performed rotating only the position of the individual pixels of the EBSD map while maintaining the original crystallographic orientations (Figure 2c). The advantage of such rotation is that we can study the effects of SPO and CPO on seismic anisotropy individually and separate the two effects. In this study, we label the models in which both pixels and crystallographic orientations are simultaneously rotated the *SPO-CPO-rotation models*, and the models in which only the pixels are rotated the *SPO-rotation models*.

2.4. Pulse Transmission Technique

The pulse transmission technique has been developed [Birch, 1960] and applied to measure seismic velocities (V_p and V_s) by using the propagation of ultrasonic waves along rock cores under various confining pressures and elevated temperatures, thus simulating in situ conditions from different depths in the Earth [e.g., Kern and Richter, 1981; Kern, 1982; Barruol and Kern, 1996; Burlini et al., 2005; Llana-Funez and Brown, 2012]. The seismic velocity can be calculated from the sample length and travel time measured by transducers located at both ends of the cored sample. From each peridotite sample, three mutually perpendicular cores (26 mm diameter, 30–50 mm length) were prepared according to macroscopically visible fabric indicators: Z cores perpendicular to the foliation, X cores parallel to the lineation, and Y cores parallel to the foliation and perpendicular to the lineation. Compressional wave velocity (V_p) measurements were performed using a hydrostatic pressure vessel applying a cycle of increasing and decreasing confining pressure with 20 MPa increments. Temperature was in equilibrium with room condition, and the source frequency was 0.1 MHz. Such pressure-temperature conditions differ from the in situ situation but remain relevant to the Earth surface and comparable with calculations as long as the elastic tensors are consistent with the

experimental conditions. The velocities measured during increasing confining pressures are always slightly lower than those during decompression, suggesting that some cracks or pore spaces did not re-open during depressurization (hysteresis). According to *Burke and Fountain* [1990], unlike depressurization, measurements made during pressurization are not reproducible. Therefore, only the V_p values measured during decompression are considered. At low confining pressure, V_p is non-linearly dependent on the confining pressure, which is interpreted to be due to closure of cracks and pores [e.g., *Birch*, 1960; *Cholach et al.*, 2005]. At higher confining pressure, the linear pressure dependency of V_p reflects the intrinsic seismic properties of the rock. For each sample, the pressure derivative was calculated using the best fit solution of the linear part of the V_p -pressure data above 100 MPa. The intrinsic velocity at room pressure (V_{p0}) is the extrapolation of this best fit solution to 0 MPa. These V_{p0} values are then used for further comparison with the numerical FE simulations and VRH estimates. The raw data from the lab are available in the supporting information.

3. Results and Interpretations

Our results of seismic velocity as a function of sample orientation can be separated into three sets, which we will compare relative to each other: (1) the Voigt and Reuss bounds and Hill estimates based on EBSD data, (2) the numerical results from FE wave propagation simulations, and (3) the experimental measurements from the laboratory.

Stereograms of seismic velocity are calculated for each mineral phase directly from the CPO data measured by EBSD (Figure 3). The bulk rock velocity stereogram results from averaging the elastic tensors for the individual mineral phases weighted by the respective mineral modal proportions. The result for the harzburgite sample ZAP205 resembles the velocity stereogram of olivine, which is the most abundant mineral phase (Figure 3, left panel). In the lherzolite sample ZAP214 (Figure 3, right panel), the bulk velocity still resembles the olivine stereogram but is overall reduced compared with sample ZAP205 due to the abundant hornblende (ca. 24%).

In a diagram of V_p versus sample orientation (or propagation direction), the results are jointly presented from numerical FE simulations, ultrasonic measurements, and the CPO-weighted bulk averages (Figure 4). Good correlation between these three data sets gives us confidence in the validity of the involved approaches, particularly the novel numerical FE technique. The curves all show the maximum and minimum V_p parallel and perpendicular to the lineation, respectively (*SPO-CPO rotation models*, Figure 4 pink squares), and the numerical FE results closely match the Hill average. With the CPO fixed relative to the propagation direction, the anisotropy is significantly reduced for sample ZAP214 and negligible for sample ZAP205 (*SPO-rotation models*, Figure 4 orange circles). The remaining anisotropy with maxima every 90° are primarily attributed to an artifact created by sampling different grains during model rotation. Any effects of SPO, which are admittedly weak in the investigated samples, should result in an orthorhombic symmetry, i.e., maxima every 180°. Thus the results confirm that the seismic velocity anisotropy is primarily controlled by CPO, while SPO only has minor effects, at least in the fracture-free model ZAP214.

Sample ZAP205 contains a fracture (Figures 1 and 2) filled with small fibers of randomly oriented serpentine. We conducted additional numerical simulations to compare a fracture-free model, assuming that the fracture is filled with the adjacent mineral phases, to a fractured model, where the fracture is filled by serpentine with an isotropic average seismic response. Generally, the velocity decreases in the fractured model (Figure 4a) due to the presence of the low-velocity serpentine and the elastic scattering at the interface between the surrounding rock material and the fracture. This velocity decrease is more significant when the fracture is perpendicular to the wave propagation direction confirming that the presence of fractures is one of the reasons for seismic anisotropy [*Guadagno and Nunziata*, 1993; *Schoenberg and Sayers*, 1995]. Furthermore, the numerically derived velocity values of the fractured model lie mostly below the Reuss (lower) bound (Figure 4a), which was derived from CPO data even considering the effect caused by the volume of serpentine. This suggests that conventional Voigt and Reuss bounds and Hill estimates can be misleading when fractures are present, which lead to a seismic velocity decrease and an anisotropy increase in an extent much exceeding their pure volume percentages, as shown by the numerical results.

The presented numerical technique provides a complementary approach to classical homogenization theories, such as Hashin-Shtrikman type average [*Castaneda and Willis*, 1995] or differential effective medium methods (DEM) [*Nishizawa and Yoshino*, 2001; *Watanabe et al.*, 2014] for seismic velocity prediction of fractured rocks.

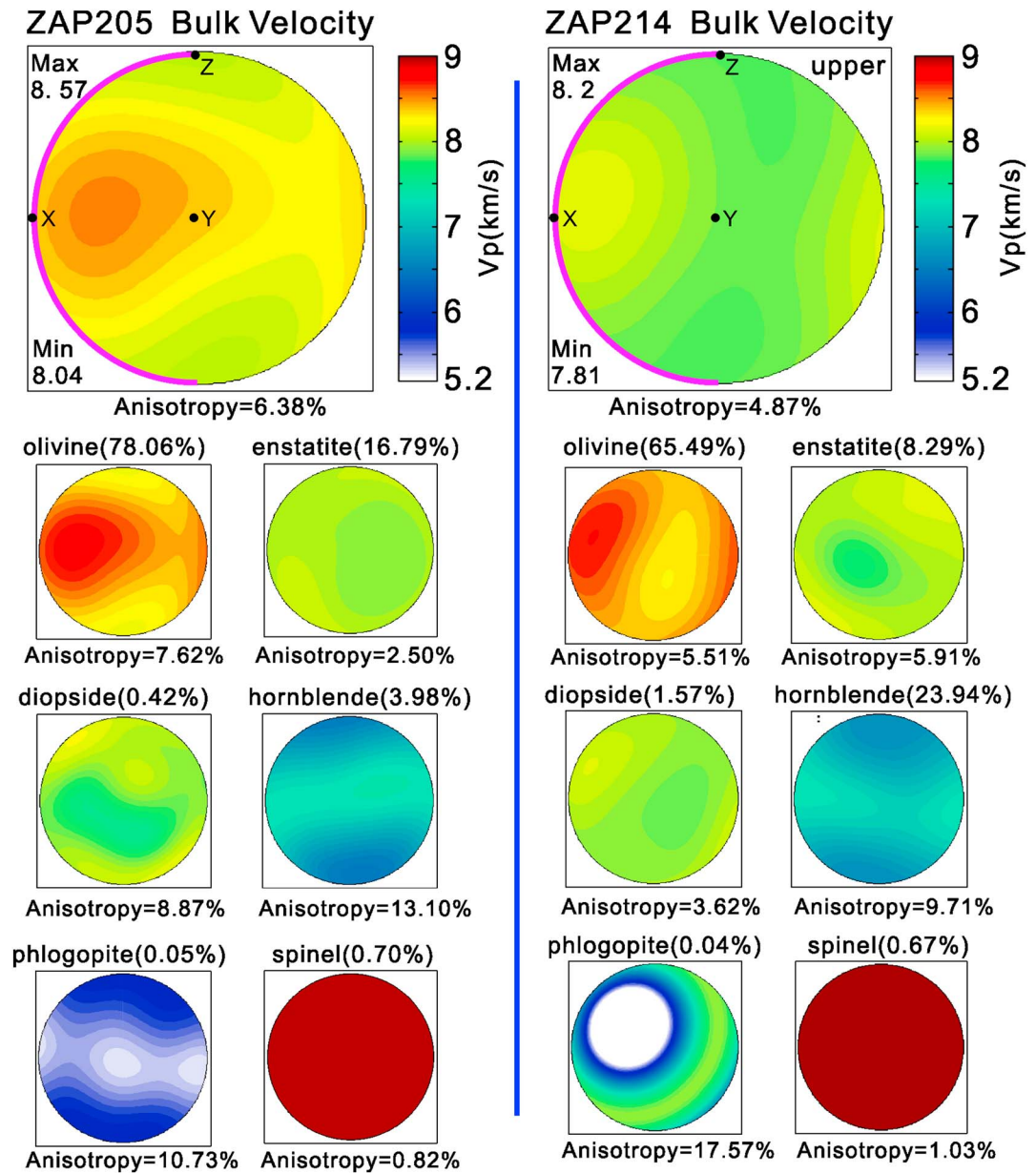


Figure 3. Calculated Hill estimate (average between Voigt and Reuss bounds) stereogram of V_p in dependence of the propagation direction derived from EBSD CPO data for sample ZAP205 (left panels) and ZAP214 (right panels). In the lower panels, modal percentage and (CPO weighted) seismic anisotropy is given for individual mineral phases; the resulting bulk velocity stereogram is shown at the top. The pink solid lines of the bulk velocity stereogram represent the measured EBSD planes, as well as the orientations for comparison with experimental velocities and numerical velocities (Figure 4). Note the difference between the hornblende modal percentages between the two samples, which slightly changes the maximal velocity orientation and reduces the value of the bulk velocity of sample ZAP214. The modal percentage of phlogopite is reduced due to the ultrapolishing for EBSD sample preparation.

4. Discussion and Implications

Our numerical FE model successfully simulates compressional wave propagation as a function of sample orientation through the fully heterogeneous and anisotropic EBSD-based 2D rock model. Here we have focused primarily on the implementation of the method of using EBSD data directly for FE modeling. We discuss potential benefits for the interpretation of the effects of CPO, SPO, and fractures on the elastic anisotropy, showing two examples of peridotite rocks. The detected seismic anisotropy in Finero peridotite is

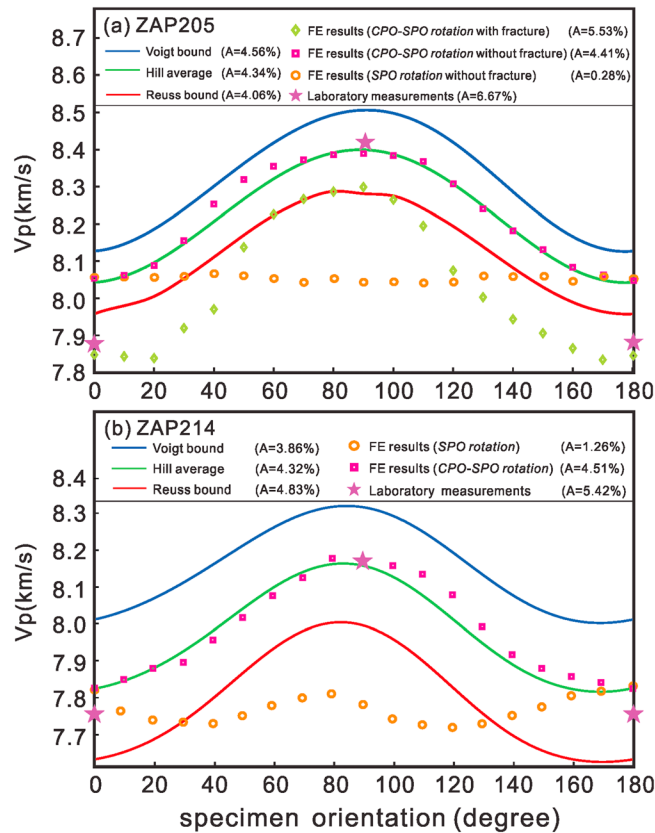


Figure 4. Seismic velocity anisotropy plot of three data sets: lines are the Voigt, Reuss, and Hill estimates extracted from the EBSD-based CPO data (Figure 3); diamonds, circles, and boxes are the numerical FE results of compressional wave propagation simulations through the 2D EBSD-based rock model; and pink stars are the laboratory measurements. The numerical results (pink boxes) show good correlation with the Hill average and with laboratory results when no fracture is present (sample ZAP214). In case of the fractured rock (sample ZAP205), numerical results are generally lower due to the low-velocity serpentine filling the fracture but follow a similar trend with orientation. In SPO-rotation models, the numerical seismic velocity exhibits dramatically less anisotropy, implying that the SPO influence is minor.

mainly caused by the CPO of olivine. If present, fractures filled with serpentine may contribute to an increase of seismic anisotropy [Dewandel *et al.*, 2003]. Abundant hornblende in sample ZAP214 is sufficient to influence the bulk rock velocity, as has also been discussed by Tatham *et al.* [2008]. The influence of SPO on the anisotropy is minor and barely distinguishable from numerical artifacts in our cases; its magnitude is less than the separation of the Voigt and Reuss bounds representing extreme cases of perfectly layered materials. Effects from SPO may become significant if the wavelength of the propagating wave is significantly shorter than the grain size, and therefore elastic scattering at mineral grain boundaries is stronger. However, shorter wavelengths also mean higher frequencies, which lie above the frequency range of any possible field application. In reality, the wavelength in most geophysical measurements (as opposed to the applied ultrasound experiments in the laboratory) is several orders of magnitude longer than the mean grain size in the peridotite, which further suppresses the significance of SPO on seismic anisotropy in a large-scale geophysical context. Our numerical results further verify the validity of conventional Voigt and Reuss bounds and the Hill average if no fractures are present, and confirm that CPO is the principle controlling factor for seismic anisotropy.

The advantage of our 2D numerical FE simulations is that the rock model represents a real heterogeneous and anisotropic microstructure scanned with the EBSD technique (animation in supporting information for wave propagation in a fractured rock). The material property at each element of the FE model is taken directly from measurements, which makes our approach distinct from statistically based homogenization theories [e.g., Mavko *et al.*, 2009]. In principle, this approach could also be combined with ray-tracing instead of FE methods, again using the EBSD map as mesh in a similar way as proposed by Epstein *et al.* [2012] for isotropic materials. However, to our knowledge there is no report so far on a successful implementation of a fully anisotropic ray-tracing scheme on such a mesh at the microscale. Typically, ray-tracing methods are applied at a much larger (crustal) scale, modeling a small number of internally homogeneous structures (layers), each of which may well have been assigned anisotropic properties derived from small-scale petrofabric analysis as discussed by Lloyd *et al.* [2011a, 2011b].

The dimension of an EBSD scan is usually limited to 2D and the size of the section cannot exceed a few centimeters in lateral direction. Besides the problem that fully 3D models would be computationally highly demanding, they are barely available in the required resolution by modern rock characterization techniques. Tomographic diffraction approaches are still limited in sample size and thus in

representative sample volume; large area serial sectioning could potentially provide some 3D orientation mapping data. This study has verified that CPO data collected from a representative 2D section are fully valid to be used for velocity estimation, as long as no major heterogeneities like fractures or highly anisotropic phases are preferentially aligned in the sample. As fractures often extend beyond the EBSD scan area, it may be favorable to capture the possible preferred fracture orientation by another imaging technique such as X-ray computer tomography. We could envision integrating the anisotropy effects of such a larger-scale fracture network with our proposed small-scale FE simulations. In this scenario, the EBSD-based FE simulations would only take care of the CPO and SPO effects, while the anisotropy effects of the inferred fracture network cover a larger scale. An upscaling procedure would combine the two scales.

Our numerical model may be extended in the future to simulate seismic wave propagation through rocks with more complex fracture geometries using a triangular numerical mesh or to model seismic attenuation by introducing visco-elastic rheology in the pore space partially filled with a fluid. The change of seismic velocity with confining pressure and temperature could as well be modeled, given that pressure and temperature derivatives of the elastic tensors of all individual mineral phases are available [Mavko et al., 2009]. Using this method, such data would allow us to precisely simulate wave propagation and investigate seismic anisotropy at different depths of the Earth, as long as real rock samples are acquired and sufficient crystallographic information is inferred. Our work may provide inspirations for further utilizing petrofabric information (like EBSD) combined with numerical simulation to better understand seismic wave propagation. Of course, future studies may extend the proposed EBSD-based FE methodology to simulate the propagation of shear waves.

5. Conclusions

We successfully applied and compared three independent methods for estimating the seismic velocity and anisotropy: laboratory measurements, velocity stereograms based on CPO-measurements using EBSD, and numerical FE wave propagation simulations. In particular the last method represents a new approach to derive elastic properties in anisotropic and heterogeneous rock models. It also allows an independent verification of CPO as the major cause of anisotropy. In the studied Finero peridotite, seismic anisotropy is a result of the CPO of dominant mineral phases (olivine for ZAP205, olivine, and hornblende for ZAP214), the presence of preferentially aligned fractures, and the SPO in this order of decreasing influence. Care has to be taken when using the Voigt, Reuss, and Hill estimates in case fractures are present as their shapes are not considered in the VRH bulk averaging scheme. The effects of fractures are larger than what is predicted simply based on their volume proportions in the bulk rock, due to strong elastic scattering and the slow velocity of fracture-filling minerals. Hydrous mineral phases can be important for seismic anisotropy only when their modal compositions are large enough compared to other abundant mineral phases (such as in sample ZAP214 with 23% hornblende). In the studied cases, phlogopite is not an important factor as its modal composition is small. The method presented in this paper offers an alternative approach to link directly EBSD data to FE simulations and potentially enables further studies focusing on highly heterogeneous and anisotropic microstructures.

Acknowledgments

This work was supported by the Swiss National Science Foundation (project UPseis, 200021_143319). We thank Dave May, Kuan Li, and Yufeng Lin who helped in the development of FE codes and cluster computation. We thank all the lab members of the Rock Deformation Lab at ETH Zurich for support in the high pressure seismic velocity measurements. We acknowledge access to the SEM-EBSD facility (Tescan EOscan) at the Laboratory of Nanometallurgy, ETH Zurich. We thank Geoffrey E. Lloyd and an anonymous reviewer for their careful and insightful review of an earlier version of this manuscript. The data to reproduce the results of this article can be found on an ETH-maintained bit-torrent server. To access the data, the software BitTorrent Sync (<http://www.bittorrent.com/sync>) has to be installed on the device of your choice and the following read-only code has to be used: BRB4M6LUBI4EVOIIFWIE2TLWBQF-NHP3T.

Michael Wyssession thanks Geoffrey Lloyd, David Wallis, and one anonymous reviewer for their assistance in evaluating this manuscript.

References

- Adams, B. L., S. I. Wright, and K. Kunze (1993), Orientation imaging: The emergence of a new microscopy, *Mater. Trans. A*, 24(4), 819–831.
- Babuska, V., and M. Cara (1991), *Seismic Anisotropy in the Earth, Modern Approaches in Geophysics*, Kluwer Academic Publishers, Dordrecht, Netherlands.
- Bachmann, F., R. Hielscher, and H. Schaeben (2010), Texture analysis with MTEX - Free and open source software toolbox, *Solid State Phenom. Ser.*, 160, 63–68.
- Barruol, G., and H. Kern (1996), Seismic anisotropy and shear-wave splitting in lower-crustal and upper-mantle rocks from the Ivrea Zone: experimental and calculated data, *Phys. Earth Planet. Inter.*, 95, 175–194.
- Bascou, J., G. Barruol, A. Vauchez, D. Mainprice, and M. Eglydio-Silva (2001), EBSD measured lattice preferred orientations and seismic properties of eclogites, *Tectonophysics*, 342, 61–80.
- Birch, F. (1960), The velocity of compressional waves in rocks to 10 kilobars, Part 1, *J. Geophys. Res.*, 65(4), 1083–1102, doi:10.1029/JZ065i004p01083.
- Burke, M., and D. Fountain (1990), Seismic properties of rocks from an exposure of extended continental crust—New laboratory measurements from the Ivrea Zone, *Tectonophysics*, 182, 119–146.
- Burlini, L., and K. Kunze (2000), Fabric and seismic properties of a calcite mylonite, *Phys. Chem. Earth*, 25, 133–139.

- Burlini, L., L. Arbaret, G. Zeilinger, and J. P. Burg (2005), High-temperature and pressure seismic properties of a lower crustal prograde shear zone from the Kohistan Arc, Pakistan, *Geol. Soc. London Spec. Publ.*, *245*, 187–202.
- Castaneda, P. P., and J. R. Willis (1995), The effect of spatial distribution on the effective behavior of composite materials and cracked media, *J. Mech. Phys. Solid*, *43*, 1919–1951.
- Cholach, P. Y., J. B. Molyneux, and D. R. Schmitt (2005), Flin Flon Belt seismic anisotropy: Elastic symmetry, heterogeneity, and shear-wave splitting, *Can. J. Earth Sci.*, *42*(4), 533–554.
- Coltorti, M., and F. Siena (1984), Mantle tectonite and fractionate peridotite at Finero (Italian Western Alps), *Neues Jahrb. Mineral. Abh.*, *149*, 225–244.
- Dewandel, B., F. Boudier, H. Kern, W. Warsi, and D. Mainprice (2003), Seismic wave velocity and anisotropy of serpentinized peridotite in the Oman ophiolite, *Tectonophysics*, *370*, 77–94.
- Epstein, M., D. Peter, and M. A. Slawinski (2012), Combining ray-tracing techniques and finite-element modelling in deformable media, *Q. J. Mech. Appl. Math.*, *65*(1), 87–112.
- Erdman, M. E., B. R. Hacker, G. Zandt, and G. Seward (2013), Seismic anisotropy of the crust: Electron-backscatter diffraction measurements from the Basin and Range, *Geophys. J. Int.*, *195*(2), 1211–1229.
- Fountain, D. (1976), The Ivrea-Verbano and Strona-Ceneri zones, Northern Italy: A cross-section of the continental crust—new evidence from seismic velocities of rock samples, *Tectonophysics*, *33*, 145–165.
- Frehner, M. (2014), Krauklis wave initiation in fluid-filled fractures by a passing body wave, *Geophysics*, *79*, T27–T35, doi:10.1061/9780784412992.011.
- Frehner, M., and S. M. Schmalholz (2010), Finite-element simulations of Stoneley guided-wave reflection and scattering at the tips of fluid-filled fractures, *Geophysics*, *75*, T23–T36, doi:10.1190/1.3340361.
- Frehner, M., S. M. Schmalholz, E. H. Saenger, and H. Steeb (2008), Comparison of finite difference and finite element methods for simulating two-dimensional scattering of elastic waves, *Phys. Earth Planet. Inter.*, *171*, 112–121.
- Frese, K., V. Trommsdorff, and K. Kunze (2003), Olivine [100] normal to foliation: Lattice preferred orientation in prograde garnet peridotite formed at high H₂O activity, Cima di Gagnone (Central Alps), *Contrib. Mineral. Petrol.*, *145*(1), 75–86.
- Guadagno, F. M., and C. Nunziata (1993), Seismic velocities of fractured carbonate rocks (southern Apennines, Italy), *Geophys. J. Int.*, *113*, 739–746.
- Hill, R. (1952), The elastic behaviour of a crystalline aggregate, *Proc. Phys. Soc.*, *65*, 349–354.
- Holbrook, W. S., W. D. Mooney, and N. I. Christensen (1992), The seismic velocity structure of the deep continental crust, *Cont. Lower Crust*, *23*, 1–43.
- Holliger, K., and A. Levander (1994), Seismic structure of gneiss/granitic upper crust geological and petrophysical evidence from the Strona-Ceneri Zone (Northern Italy) and implications for crustal seismic exploration, *Geophys. J. Int.*, *119*(2), 497–510.
- Holliger, K., A. R. Levander, and J. A. Goff (1993), Stochastic modeling of the reflective lower crust: Petrophysical and geological evidence from the Ivrea Zone (northern Italy), *J. Geophys. Res.*, *98*(B7), 11,967–11,980, doi:10.1029/93JB00351.
- Ismail, W. B., and D. Mainprice (1998), An olivine fabric database: an overview of upper mantle fabrics and seismic anisotropy, *Tectonophysics*, *296*, 145–157.
- Kern, H. (1982), Elastic-wave velocity in crustal and mantle rocks at high pressure and temperature: The role of the high-low quartz transition and of dehydration reactions, *Phys. Earth Planet. Inter.*, *20*, 12–23.
- Kern, H., and A. Richter (1981), Temperature derivatives of compressional and shear wave velocities in crustal and mantle rocks at 6 kbar confining pressure, *J. Geophys.*, *49*, 47–56.
- Khazanehdari, J., E. H. Rutter, and K. H. Brodie (2000), High pressure/temperature seismic 696 velocity structure of the mid- and lower-crustal rocks of the Ivrea-Verbano zone and Serie dei Laghi, N.W. Italy, *J. Geophys. Res.*, *105*(B6), 13,843–13,858, doi:10.1029/2000JB900025.
- Lensch, G. (1968), Die Ultramafite der Zone von Ivrea und ihre geologische Interpretation, *Schweiz. Mineral. Petrogr. Mitt.*, *48*, 91–102.
- Llana-Funez, S., and D. Brown (2012), Contribution of crystallographic preferred orientation to seismic anisotropy across a surface analog of the continental Moho at Cabo Ortegal, Spain, *Geol. Soc. Am. Bull.*, *124*, 1495–1513.
- Llana-Funez, S., D. Brown, R. Carbonell, J. Alvarez-Marron, and M. Salisbury (2009), Seismic anisotropy of upper mantle-lower continental crust rocks in Cabo Ortegal (NW Spain) from crystallographic preferred orientation (CPO) patterns, *Trabajos de Geol.*, *29*, 432–436.
- Lloyd, G. E., and J. M. Kendall (2005), Petrofabric-derived seismic properties of a mylonitic quartz simple shear zone: Implications for seismic reflection profiling, *Geol. Soc. London Spec. Publ.*, *240*, 75–94.
- Lloyd, G. E., J. M. Halliday, R. W. H. Butler, M. Casey, J.-M. Kendall, J. Wookey, and D. Mainprice (2011a), From crystal to crustal: Petrofabric-derived seismic modelling of regional tectonics, *Geol. Soc. London Spec. Publ.*, *360*, 49,078.
- Lloyd, G. E., R. W. H. Butler, M. Casey, D. J. Tatham, and D. Mainprice (2011b), Constraints on the seismic properties of the middle and lower continental crust. Deformation Mechanisms, Rheology and Tectonics: Microstructures, Mechanics and Anisotropy, *Geol. Soc. London Spec. Publ.*, *360*, 7–32.
- Mainprice, D. (1990), A Fortran program to calculate seismic anisotropy from the lattice preferred orientation of minerals, *C. R. Geosci.*, *16*(3), 385–393.
- Mainprice, D., and M. Humbert (1993), Methods of calculating petrophysical properties from lattice preferred orientation data, *Surv. Geophys.*, *15*, 575–592.
- Mainprice, D., R. Hielscher, and H. Schaeben (2011), Calculating anisotropic physical properties from texture data using the MTEX open source package, *Geol. Soc. London Spec. Publ.*, *360*, 175–192.
- Mauler, A., L. Burlini, K. Kunze, P. Philippot, and J.-P. Burg (2000), P-wave anisotropy in eclogites and relationship to the omphacite crystallographic fabric, *Phys. Chem. Earth*, *25*(2), 119–126.
- Mavko, G., T. Mukerji, and J. Dvorkin (2009), *The Rock Physics Handbook*, Cambridge Univ. Press, Cambridge, U. K.
- Naus-Thijssen, F. M. J., A. J. Goupee, S. E. Johnson, S. S. Vel, and C. Gerbi (2011), The influence of crenulation cleavage development on the bulk elastic and seismic properties of phyllosilicate-rich rocks, *Earth Planet. Sci. Lett.*, *311*, 212–224.
- Nicolas, A., and N. I. Christensen (1987), Formation of anisotropy in uppermantle peridotites—A review, in *The Composition, Structure and Dynamics of the Lithosphere-Asthenosphere System*, *Geodyn. Ser.*, vol. 16, edited by C. Froidevaux and K. Fuchs, pp. 111–123, AGU, Washington D. C.
- Nishizawa, O., and T. Yoshino (2001), Seismic velocity anisotropy in mica-rich rocks: An inclusion model, *Geophys. J. Int.*, *145*(1), 19–32.
- Pera, E., D. Mainprice, and L. Burlini (2003), Anisotropic seismic properties of the upper mantle beneath the Torre Alfina area (Northern Apennines, Central Italy), *Tectonophysics*, *370*, 11–30.
- Prior, D. J., et al. (1999), The application of electron backscatter diffraction and orientation contrast imaging in the SEM to textural problems in rocks, *Am. Mineral.*, *84*, 1741–1795.

- Reuss, A. (1929), Berechnung der Fließgrenze von Mischkristallen auf Grund der Plastizitätsbedingung für Einkristalle, *Z. Angew. Math. Mech.*, *9*, 49–58.
- Rudnick, R. L., and D. M. Fountain (1995), Nature and composition of the continental crust: A lower crustal perspective, *Rev. Geophys.*, *33*(3), 267–309, doi:10.1029/95RG01302.
- Rutter, E. H., J. Khazanehdari, K. H. Brodie, D. J. Blundell, and D. A. Waltham (1999), Synthetic seismic reflection profile through the Ivrea zone—Serie dei Laghi continental crustal section, northwestern Italy, *Geology*, *27*, 79–82.
- Rutter, E., K. Brodie, T. James, and L. Burlini (2007), Large-scale folding in the upper part of the Ivrea-Verbano zone, NW Italy, *J. Struct. Geol.*, *29*, 1–17.
- Schoenberg, M., and C. Sayers (1995), Seismic anisotropy of fractured rock, *Geophysics*, *60*, 204–211.
- Schwartz, A. J., M. Kumar, and B. L. Adams (2009), *Electron Backscatter Diffraction in Materials Science*, Springer, New York, doi:10.1007/978-0-387-88136-2.
- Siena, F., and M. Coltorti (1989), The petrogenesis of a hydrated mafic ultramafic complex and the role of amphibole fractionation at Finero (Italian Western Alps), *Neues Jahrb. Mineral. Monatsh.*, *6*, 255–274.
- Tatham, D. J., G. E. Lloyd, R. W. H. Butler, and M. Casey (2008), Amphibole and lower crustal seismic properties, *Earth Planet. Sci. Lett.*, *267*, 118–128.
- Valcke, S. L. A., M. Casey, G. E. Lloyd, J. M. Kendal, and Q. J. Fisher (2006), Lattice preferred orientation and seismic anisotropy in sedimentary rocks, *Geophys. J. Int.*, *166*, 652–666.
- Voigt, W. (1928), *Lehrbuch der Kristalphysik*, Teubner, Leipzig, Germany.
- Wang, Q., L. Burlini, D. Mainprice, and Z. Xu (2009), Geochemistry, petrofabrics and seismic properties of eclogites from the Chinese Continental Scientific Drilling boreholes in the Sulu UHP terrane, eastern China, *Tectonophysics*, *475*, 251–266.
- Watanabe, T., Y. Shirasugi, and K. Michibayashi (2014), A new method for calculating seismic velocities in rocks containing strongly dimensionally anisotropic mineral grains and its application to antigorite-bearing serpentinite mylonites, *Earth Planet. Sci. Lett.*, *391*, 24–35.
- Worthington, J. R., B. R. Hacker, and G. Zandt (2013), Distinguishing eclogite from peridotite: EBSD-based calculations of seismic velocities, *Geophys. J. Int.*, *193*(1), 489–505.
- Xu, Z. Q., Q. Wang, S. C. Ji, J. Chen, L. S. Zeng, J. S. Yang, F. Y. Chen, F. H. Liang, and H. R. Wenk (2006), Petrofabrics and seismic properties of garnet peridotite from the UHP Sulu terrane (China): Implications for olivine deformation mechanism in a cold and dry subducting continental slab, *Tectonophysics*, *421*, 111–127.